



**HAL**  
open science

# Isotropic and anisotropic collision-induced light scattering spectra of krypton gas simultaneously fitted by ground state interatomic potential

Jean-Luc Godet, M.S.A. El-Kader

► **To cite this version:**

Jean-Luc Godet, M.S.A. El-Kader. Isotropic and anisotropic collision-induced light scattering spectra of krypton gas simultaneously fitted by ground state interatomic potential. *Journal of Quantitative Spectroscopy and Radiative Transfer*, 2022, 288, pp.108251. 10.1016/j.jqsrt.2022.108251 . hal-04085838

**HAL Id: hal-04085838**

**<https://univ-angers.hal.science/hal-04085838>**

Submitted on 22 Jul 2024

**HAL** is a multi-disciplinary open access archive for the deposit and dissemination of scientific research documents, whether they are published or not. The documents may come from teaching and research institutions in France or abroad, or from public or private research centers.

L'archive ouverte pluridisciplinaire **HAL**, est destinée au dépôt et à la diffusion de documents scientifiques de niveau recherche, publiés ou non, émanant des établissements d'enseignement et de recherche français ou étrangers, des laboratoires publics ou privés.



Distributed under a Creative Commons Attribution - NonCommercial 4.0 International License

# Isotropic and Anisotropic Collision-Induced Light Scattering Spectra of Krypton Gas Simultaneously Fitted by Ground State Interatomic Potential

J.-L. Godet <sup>a\*</sup>, M.S.A. El-Kader <sup>b\*\*</sup>

<sup>a</sup> *Laboratoire de photonique d'Angers (LPHIA), Université d'Angers, 2 boulevard Lavoisier, 49045 Angers, France*

<sup>b</sup> *Department of Engineering Mathematics and Physics, Faculty of Engineering, Cairo University, Giza, 12211, Egypt*

## Keywords

Krypton, Interatomic potential, CILS, Pair polarizability,

## Abstract

Isotropic and anisotropic binary collision-induced light scattering spectra of gaseous krypton obtained at room temperature are analyzed in terms of different interatomic potentials, both reference and recent, and trace and anisotropy models of interaction-induced polarizability. The spectral intensities obtained numerically at low frequencies are determined by bound and free transitions. At intermediate and high frequencies, the spectra are sensitive to both the attractive part of the potential and to short-range values of the trace or anisotropy. An empirical interatomic potential for the krypton gas interaction is developed by simultaneously fitting the Barker et al. (BFW) and modified Tang-Toennies (MTT) potentials to thermophysical and transport properties over a wide temperature range. The quality of the present potentials was checked by comparison between the calculated and experimental vibrational energy levels. The results show that these are the most accurate potentials reported to date for this system, both for the reproduction of spectral line shapes and spectral moments.

---

\* Corresponding author: jean-luc.godet@univ-angers.fr

\*\* mohamedsay68@eng.cu.edu.eg

## 1. Introduction

Collision-induced light scattering (CILS) spectra that are scattered by a dense fluid or gas have a power spectrum which is shaped by two functions of the intermolecular separation  $r$ : the interaction potential  $V(r)$ , and, respectively, the trace  $\alpha(r)$  and anisotropy  $\beta(r)$  of the induced polarizability tensor of the interacting pair of atoms or molecules [1–4]. Recently, detailed analysis of the bulk properties of hydrogen, nitrogen, methane and of the inert gases helium, neon, argon, krypton, xenon, and mixtures has led to accurate estimates of the pair potential for the interaction of ground-state atoms and molecules [5–15]. These estimates have been confirmed rather dramatically by experimental data on the spectra of gas dimers and on the differential and total scattering cross sections of molecular beams [16–18]. In particular, the different interatomic potentials [5–15] determined from the second pressure virial coefficients, viscosity, thermal conductivity, diffusion coefficients and thermal diffusion factors provided a very satisfactory verification of all the experimental data and methods of analysis.

From this point of view, no accurate potential is available for krypton. We calculate an approximate interatomic potential for the krypton interaction using mostly the methods outlined in previous papers [8–15]. Since the details of the methods are given there and the references therein, we will only restate the equations when it is necessary for the sake of continuity. To reiterate, the basic strategy in this paper is to include isotropic and anisotropic light scattering data (CILS) in addition to the data on thermo-physical, transport and spectroscopic properties to fit the Barker, Fisher and Watts (BFW) and Modified Tang-Toennies (MTT) potential models for interatomic krypton interactions.

Different experiments are sensitive to different regions of the interatomic potential. Collision-induced light scattering (CILS) intensities are most sensitive to the attractive potential from  $r_m$  at which the potential has its minimum out to the asymptotic long range region, and the rainbow and supernumerary oscillations give detailed information about that part of the potential [18]. The pressure virial coefficients reflect the size of  $r_m$  and the volume of the attractive well [19]. The viscosity, self-diffusion, thermal conductivity and thermal diffusion factors data are most sensitive to the wall of the potential from  $r_m$  inward to a point where the potential is repulsive [20]. Thus, these six properties with the spectroscopic data can, in principle, be used to develop a potential over a fairly broad range of interatomic distances.

The paper is organized as follows: the interatomic potential models adopted from multiproperty analysis are presented in Sections 2 and 3. The analysis of the theoretical method for calculating the parameters of the trace and anisotropy models of the pair-polarizability is given in Section 4. The light scattering induced by collision of two krypton atoms is briefly given in Section 5, together with the computational implementation. Results are discussed in the same Section 5 and the concluding remarks are given in the last Section.

## 2. The interatomic potentials and multi-property analysis

The interatomic potentials we provide here is obtained through the analysis of the pressure second virial coefficients [21-35] and a set of gaseous transport properties [36-63] and spectroscopic properties [64-69]. For the analysis of all these experimental data, we consider the BFW and MTT interatomic potentials which in all region of interactions can be represented by the following formula:

- for the BFW potential [70],

$$V(r) = \varepsilon \sum_{i=0}^5 A_i (x-1)^i \exp(\xi(1-x)) - \sum_{n=3}^{\infty} \frac{C_{2n}}{r^{2n} + dr_m^{2n}}, \quad (1)$$

where  $x=r/r_m$  is the reduced distance,  $\varepsilon$  is the potential depth,  $r_m$  is the distance at the minimum potential and the rest ( $\xi, \delta$ ) are fitting parameters;

- for the MTT potential [71],

$$V(r) = Ar^{\left(\frac{7}{2B}-1\right)} \exp(-2B r) - \sum_{n=3}^{\infty} \frac{C_{2n} f_{2n}(r)}{r^{2n}} \quad (2)$$

where the  $f_{2n}(r)$  are the appropriate damping functions, given by the expression derived by Tang and Toennies [72]

$$f_{2n}(r) = 1 - \exp(-b(r)) \sum_{k=0}^{2n} \frac{[b(r)]^k}{k!} \quad (3)$$

and

$$b(r) = 1 - \frac{7}{2B} + 2B r \quad (4)$$


Even at the present (BFW) level, there are really thirteen parameters ( $\varepsilon, r_m, A_0, A_1, A_2, A_3, A_4, A_5, \xi, \delta, C_6, C_8, C_{10}$ ) and in the (MTT) level, there are seven free parameters ( $\varepsilon, r_m, A, \mathfrak{B}, C_6, C_8, C_{10}$ ) which are far too many to determine from the present data. Accordingly we proceeded as follows: the coefficients  $A_0, A_1, A$  and  $\mathfrak{B}$  are determined from the conditions of continuity and the long-range dispersion coefficients were taken from theoretical calculations of Fransson et al. [73] for  $C_6$  and Thakkar et al. [74] for  $C_8$  and  $C_{10}$ , leaving rest parameters in these models that were varied to fit the second pressure virial coefficient,  $B$ . This minimization is further supported by calculating  $\delta_\eta, \delta_\lambda, \delta_D, \delta_{\alpha_{iso}},$  and  $\delta_v$  the rms deviations calculated from viscosity, thermal conductivity, diffusion coefficients, thermal diffusion factor and vibrational energy levels, respectively. This decision leads to the potentials parameters in Table 1 as our best estimate of interatomic potentials.

**Table 1.** Parameters of the different interatomic potentials and the associated values of  $\delta_j$ .

For krypton interactions,  $\epsilon=0.01$ . Besides,  $\delta_j$  is defined by,  $\delta_j^2 = \frac{1}{n_j} \sum_{i=1}^{n_j} \Delta_{ji}^{-2} (P_{ji} - p_{ji})^2$

where  $P_{ji}$  and  $p_{ji}$  are, respectively, the calculated and experimental values of property  $j$  at a temperature  $i$  and  $\Delta_{ji}$  is the corresponding experimental uncertainty. The subscripts B,  $\eta$ ,  $\lambda$ , D,  $\alpha_{iso}$  and V refer, respectively, to the interaction second pressure virial coefficient, viscosity, thermal conductivity, diffusion coefficient, thermal diffusion factor and vibrational energy levels.

The overall rms deviation was obtained from  $\delta_o = \sqrt{\frac{1}{N} (\sum_{j=1}^N \delta_j^2)}$ , with  $N=6$ .

Pots.	$\epsilon/k_B[K]$	$r_m[\text{\AA}]$	$\sigma[\text{\AA}]$	$\xi$	$A_0$	$A_1$	$A_2$	$A_3$	$A_4$	$A_5$	A	
BFW	201.0	4.015	3.59	9.3	1.08538	-4.98471	10.8602	-23.0	9.5	-36.0	-	-
MTT	201.2	4.0175	3.584	-	-	-	-	-	-	-	51.3221	1.05587
	$\delta_B$	$\delta_\eta$	$\delta_\lambda$	$\delta_D$	$\delta_{\alpha_{iso}}$	$\delta_V$	$\delta_o$					
BFW	0.68	0.43	0.67	0.71	0.89	0.24	0.64					
MTT	0.57	0.49	0.69	0.73	0.87	0.18	0.63					

### 3. Multi-property Analysis

In this section the calculations of the experimental quantities are described. The Monchick-Mason approximation [75] which neglects the effect of inelastic transitions on the relative kinetic energy is applied in the computations of the thermo-physical and transport properties.

#### 3.1 Analysis of pressure second virial coefficients

An effective means for checking the validity of the different potential parameters can be made using the second pressure virial coefficient data [21-35] at different temperatures. The interaction second pressure virial coefficient B at temperature T was calculated classically with the first three quantum corrections from [76]:

$$B(T) = B_{cl}(T) + \lambda B_{qm,1}(T) + \lambda^2 B_{qm,2}(T) + \lambda^3 B_{qm,3}(T) \quad (5)$$

where

$$B_{cl}(T) = 2\pi N_o \int_0^\infty [1 - \exp(-V(r)/k_B T)] r^2 dr \quad (6)$$

and the first three quantum corrections  $B_{qm,1}(T)$ ,  $B_{qm,2}(T)$  and  $B_{qm,3}(T)$  are given in Ref.[76], with,  $\lambda = \hbar^2/(12mk_B T)$ ,  $\hbar = h/2\pi$ ,  $m$  and  $N_o$  are the atomic mass and Avogadro's number. The calculated B including the first three quantum corrections were compared with the experimental results [21-35] which are seen in Table 1 and Fig. 1.

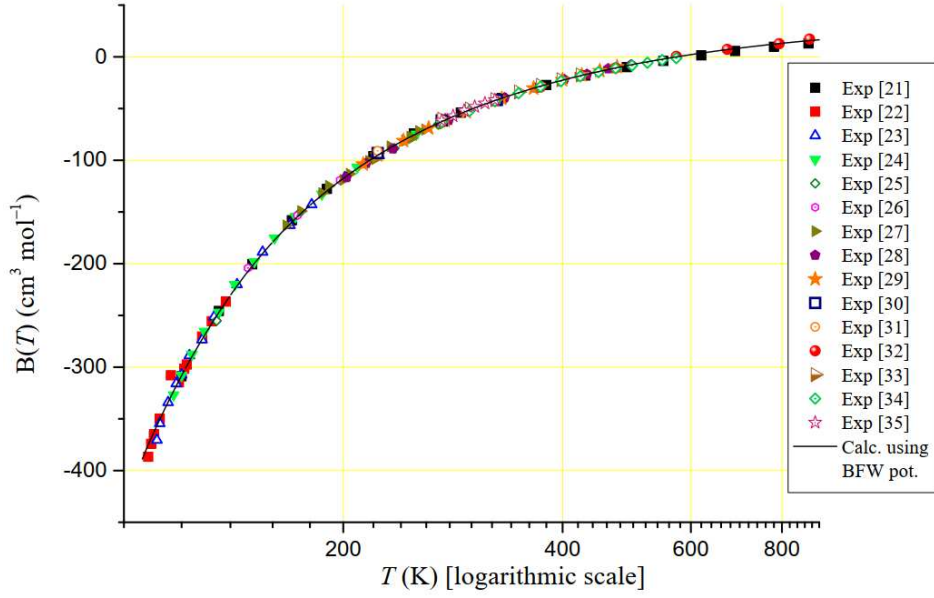


**Fig. 1.** Temperature dependence of the Krypton gas interaction pressure second virial coefficients  $B$  in  $\text{cm}^3 \text{mol}^{-1}$  versus temperature in K. Comparison is made with previously available experimental results [21-35]. The calculations were performed using the present BFW interatomic potential.

### 3.2 Analysis of traditional transport properties

An additional check on the proposed potential consists of the calculation of the transport properties i.e. viscosity  $\eta$ , thermal conductivity  $\lambda$ , diffusion coefficient  $D$  and thermal diffusion factor  $\alpha_{\text{iso}}$  at different temperatures of Krypton. These are obtained via the formulae of Monchick et al. [75] and their comparison to the accurate experimental and theoretical results [36-63] which are clear by calculating the associated values of  $\delta_j$  as shown in Table 1. The agreements for this system under consideration are excellent in the whole temperature range.

In this respect, according to the kinetic theory of gases at low density and the Chapman-Enskog solution of the Boltzmann equation, the transport properties can be expressed with the help of a series of collision integrals that depend on the intermolecular potential energy and are defined as: [77]

$$\theta = \pi - 2b \int_{r_0}^{\infty} \frac{dr}{r^2 (1 - (b/r)^2 - (V(r)/E))^{1/2}} \quad (7)$$

$$Q^{(l)}(E) = 2\pi \left( 1 - \frac{1 + (-1)^l}{2(1+l)} \right)^{-1} \int_0^{\infty} (1 - \text{Cos}^l \theta) b db \quad (8)$$

$$\Omega^{(l,s)}(T) = \left( (s+1)! (k_B T)^{s+2} \right)^{-1} \int_0^{\infty} Q^{(l)}(E) \exp(-E/k_B T) E^{s+1} dE \quad (9)$$

where  $\theta$  is the scattering angle,  $Q^{(l)}(E)$ , the transport collision integral,  $b$ , the impact parameter,  $E$ , the relative kinetic energy of colliding atoms and  $r_0$ , the closest approach of two atoms. Thus, three successive numerical integrations are required to obtain a collision integral. The reduced collision integral is defined by

$$\Omega^{*(l,s)}(T) = \frac{\Omega^{(l,s)}(T)}{\pi\sigma^2} \quad (10)$$

Where  $\sigma$  is the length scaling factor such that  $V(\sigma)=0$ .

The potential energy would serve as the input information required in calculating the collision integrals and consequently the transport properties. Kinetic-theory expressions for the transport properties (viscosity, thermal conductivity, diffusion coefficient and thermal diffusion factor) in terms of the collision integrals for the binary gas are given by the following equations: [48]

$$\eta_{12} = \frac{5}{16} \left( \frac{2M_1M_2 k_B T}{\pi(M_1 + M_2)} \right)^{1/2} \frac{1}{\sigma^2 \Omega^{*(2,2)}(T^*)} \quad (11)$$

$$\lambda_{12} = \frac{75}{64} \left( \frac{(M_1 + M_2) k_B^3 T}{2\pi M_1 M_2} \right)^{1/2} \frac{1}{\sigma^2 \Omega^{*(2,2)}(T^*)} \quad (12)$$

$$D = \frac{3}{8} \left( \frac{(M_1 + M_2) k_B^3 T^3}{2\pi M_1 M_2} \right)^{1/2} \frac{(1 + \Delta)}{P \sigma^2 \Omega^{*(1,1)}(T^*)} \quad (13)$$

$$\alpha_{\text{iso}} = (6C_{12}^* - 5) \left( \frac{x_1 S_1 - x_2 S_2}{x_1^2 Q_1 + x_2^2 Q_2 + x_1 x_2 Q_{12}} \right) (1 + K_2) \quad (14)$$

with the molecular weights  $M_1$  and  $M_2$  in grams, the pressure  $P$  in atm and the reduced temperature  $T^* = T/\epsilon$ . The expressions for the second-order correction  $\Delta$  as well as the values of  $C_{12}^*$ ,  $S$  and  $Q$  are listed in Appendix C of Ref. [48]. The correction term  $K_2$  is small in magnitude and may be neglected in the present calculations.

### 3.3 Vibrational Energy Spacings

With the above obtained interaction potentials the vibrational energy spacings can be calculated by solving the radial one-dimensional Schrödinger equation. In the present paper this equation is solved numerically. The interaction potentials of Kr with the internuclear separation between 3.0 a.u. and 200 a.u. are used to do the calculation. The size of the grid points is 1600. Table 2 presents the calculation results for krypton dimers. It is seen from Table 2 that the agreement of the two sets of spacings predicted by the MTT and BFW is good.

The experimental and other theoretical results are also listed in the Table 2 for comparison [64-69]. It is gratifying to find that the spacings of the homonuclear rare-gas dimers predicted by the MTT and BFW potential models are in excellent agreement with the experimental results if the experimental error bar are taken into consideration.

**Table 2:** Comparison of our computed vibrational energy spacings for Kr gas dimers with experimental and other theoretical data. All values are given in  $\text{cm}^{-1}$ .

Transition	MTT	BFW	Sheng [66]	Jäger [67]	Ogilvie [68]	Aziz [65]	Waldrop [64]	Exp. [69]
0-1	21.52	21.49	21.2633	21.434	21.53	21.41	21.466±0.081	21.56±0.54
1-2	19.32	19.23	19.1528	19.26	19.38	19.3	19.307±0.077	19.09±0.57
2-3	17.12	17.03	17.0580	17.105	17.22	17.2	17.166±0.073	16.76±0.60
3-4	14.98	14.89	14.988	14.979	15.07	15.11	15.053±0.069	14.76±0.75
4-5	12.89	12.81	12.9590	12.897	12.95	13.02	12.98±0.065	12.23±0.51
5-6	10.87	10.83	10.9900	10.875	10.9	10.97	10.963±0.062	10.49±0.50
6-7	8.94	8.92	9.0954	8.938	8.95	9.01	9.026±0.06	8.92±0.44
7-8	7.14	7.13	7.2952	7.117	7.14	7.17	7.199±0.063	6.92±0.63
8-9	5.49	5.48	5.6228	5.445	5.48	5.49	5.517±0.064	5.54±0.30

#### 4. Analysis of CILS spectral moments to determine the trace $\alpha(r)$ and anisotropy $\beta(r)$

The method of detailed analysis of the first three even moments of the depolarized light scattering spectrum (CILS) has been used by Barocchi-Zoppi [78,79], and Chrysos-Dixneuf [80-82] for the determination of the extra-dipole-induced dipole (EDID) contribution to the pair-polarizability anisotropy of neon and argon. This consists of establishing an appropriate parameterized model form for anisotropy and then searching by means of a computer for the sets of parameters that are consistent with the experimental values of the moments.

For the sake of comparison and discussion, for the present calculations we considered three models of the pair-polarizability trace and anisotropy which are:

- the two-term dipole-induced dipole models (DID), [83]

$$\alpha(r) = \frac{4\alpha_0^3}{r^6} + \frac{4\alpha_0^4}{r^9} \quad (15)$$

$$\beta(r) = \frac{6\alpha_0^2}{r^3} + \frac{6\alpha_0^3}{r^6} \quad (16)$$

where  $\alpha_0$  is the polarizability of the individual isolated atoms;



- the ab initio self-consistent field (SCF) and the second-order Møller–Plesset (MP2) trace and anisotropy polarizability models of Maroulis; [84]
- the analytical models of Buckingham *et al.* [85], hereafter referred to as parameterized models (PM), [86-88]

$$\alpha(r) = \left( 4\alpha_0^3 + \frac{5\gamma C_6}{9\alpha_0} \right) \frac{1}{r^6} + \frac{20\alpha_0^2 C}{r^8} - g_1 \exp\left( -\frac{r-\sigma}{r_1} \right) \quad (17)$$

$$\beta(r) = \frac{6\alpha_0^2}{r^3} + \left( 6\alpha_0^3 + \frac{\gamma C_6}{3\alpha_0} \right) \frac{1}{r^6} + \frac{24\alpha_0^2 C}{r^8} - g_2 \exp\left( -\frac{r-\sigma}{r_2} \right). \quad (18)$$

Here,  $\alpha_0$  and  $\gamma$  designate atomic polarizability and hyperpolarizability respectively,  $C_6$  is the dispersion force coefficient and  $C$  is the quadrupole polarizability. The values of the parameters used for the pair Kr-Kr are given in Table 3.

**Table 3.** Experimental and fitted parameters used in Eqs. (17, 18) for the pair Kr-Kr (atomic units).

$\alpha$	$C_6$	$C$	$\gamma$	$g_1$	$r_1$	$g_2$	$r_2$	$\sigma$	(au)
17.26 <sup>a</sup>	136 <sup>a</sup>	95.02 <sup>b</sup>	2233.0 <sup>b</sup>	0.5159	0.9189	0.9448	0.6055	6.784	

a: Ref.[73] for ADC(3/2); b: Ref.[84];

We shall use Eqs. (17-18) below to see if the trace and anisotropy can be approximated by such simple models which will be seen to provide a useful empirical basis to describe diatom polarizabilities.

In order to make the presentation of our results to be comparable with those given by other authors, it is convenient to rewrite  $\alpha(r)$  and  $\beta(r)$  of Eqs.(17-18) in terms of the reduced variable  $x = r/r_m$  where  $r_m$  is the separation at the minimum of the interatomic potential  $V(r)$ . In this case,

$$\alpha(x) = (A_6^* x^{-6} + B_1^* x^{-8} - g_1^* \exp(-\frac{x-\sigma^*}{x_1})) \quad (19)$$

$$\beta(x) = \frac{6\alpha_0^2}{r_m^3} (x^{-3} + A^* x^{-6} + B_2^* x^{-8} - g_2^* \exp(-\frac{x-\sigma^*}{x_2})) \quad (20)$$

where

$$A_6^* = (4\alpha_0^3 + \frac{5}{9}\gamma C_6/\alpha_0)/r_m^6; \quad B_1^* = 20\alpha_0^2 C/r_m^8; \quad g_1^* = g_1; \quad x_1 = r_1/r_m; \quad \sigma^* = \sigma$$

$$A^* = (6\alpha_0^3 + \gamma C_6/3\alpha_0)/6\alpha_0^2 r_m^3; \quad B_2^* = 4C/r_m^5; \quad g_2^* = g_2 r_m^3/6\alpha_0^2 \quad \text{and} \quad x_2 = r_2/r_m.$$

The substitutions of Eq. (19) into the moment expressions of Moraldi, [89] with  $L=0$  for the isotropic spectrum, and of Eq. (20) into the same expressions, with  $L=2$  for the anisotropic spectrum, make it possible to rewrite them in the form of quadratic equations for the unknown  $g_1^*$  and  $g_2^*$  with coefficients which are parametric functions of  $x_1$  and  $x_2$ . The equations those one obtains from the moments of the isotropic and anisotropic spectra respectively are of the form:

$$Y_{i+1} = Y_i - D_1^i \Big|_{y_i} F(Y_i) \quad (21)$$

$$Z_{i+1} = Z_i - D_2^i \Big|_{z_i} F(Z_i) \quad (22)$$

where the Jacobian matrices are given by

$$D_1(Y) = \begin{pmatrix} \frac{\partial M_0^{iso}}{\partial B_1} & \frac{\partial M_0^{iso}}{\partial g_1} & \frac{\partial M_0^{iso}}{\partial r_1} \\ \frac{\partial M_1^{iso}}{\partial B_1} & \frac{\partial M_1^{iso}}{\partial g_1} & \frac{\partial M_1^{iso}}{\partial r_1} \\ \frac{\partial M_2^{iso}}{\partial B_1} & \frac{\partial M_2^{iso}}{\partial g_1} & \frac{\partial M_2^{iso}}{\partial r_1} \end{pmatrix}, \quad (23)$$

$$D_2(Z) = \begin{pmatrix} \frac{\partial M_0^{aniso}}{\partial B_2} & \frac{\partial M_0^{aniso}}{\partial g_2} & \frac{\partial M_0^{aniso}}{\partial r_2} \\ \frac{\partial M_1^{aniso}}{\partial B_2} & \frac{\partial M_1^{aniso}}{\partial g_2} & \frac{\partial M_1^{aniso}}{\partial r_2} \\ \frac{\partial M_2^{aniso}}{\partial B_2} & \frac{\partial M_2^{aniso}}{\partial g_2} & \frac{\partial M_2^{aniso}}{\partial r_2} \end{pmatrix} \quad (24)$$

and the two column vectors  $Y$  and  $F(Y)$  for isotropic moments and  $Z$  and  $F(Z)$  for anisotropic moments are defined as

$$Y = \begin{pmatrix} B_1 \\ g_1 \\ r_1 \end{pmatrix}, \quad (25)$$

$$F(Y) = \begin{pmatrix} \Delta M_0^{iso} \\ \Delta M_1^{iso} \\ \Delta M_2^{iso} \end{pmatrix}, \quad (26)$$

$$Z = \begin{pmatrix} B_2 \\ g_2 \\ r_2 \end{pmatrix}, \quad (27)$$

$$F(Z) = \begin{pmatrix} \Delta M_0^{aniso} \\ \Delta M_1^{aniso} \\ \Delta M_2^{aniso} \end{pmatrix}, \quad (28)$$

where  $\Delta M_n$  are the difference between theoretical and experimental moments of the isotropic and anisotropic light scattering spectra.

Once convergences are obtained, the column vectors solutions  $\bar{Y}$  and  $\bar{Z}$  have to satisfy  $F(\bar{Y}) = 0$  for the isotropic moments and  $F(\bar{Z}) = 0$  for the anisotropic moments. Each element of the matrices  $D_1$  and  $D_2$  reads

$$(D_1)_{ab} = 4\pi \int_0^{\infty} a_{ab}(Y) \exp(-V(r)/k_B T) r^2 dr \quad (29)$$

$$(D_2)_{ab} = 4\pi \int_0^{\infty} b_{ab}(Z) \exp(-V(r)/k_B T) r^2 dr \quad (30)$$

where  $a, b=1, 2$  and  $3$  stand for the line and column numbers of the matrices  $D_1$  and  $D_2$  respectively. For the specific functional forms of  $\alpha(r)$  and  $\beta(r)$  given by Eqs. (17-18), the nine elements  $a_{ab}(Y)$  and  $b_{ab}(Z)$  are calculated.

The great advantages of this method for calculating the parameters of the models for  $\alpha(r)$  and  $\beta(r)$  are the speed of computation and that the trial-and-error approach is avoided. The method of moments analysis has been applied to the collision-induced light scattering (CILS) spectra of Ne, Ar, Kr, Xe and CH<sub>4</sub> [81, 82, 86, 90]. Because the correction to the first-order DID expression is quite small over most of the interatomic separations probed by the atomic motions, and the two correction terms to a large extent cancel out the effects of each other, the numerical values derived for the parameters  $g_1$  of the trace and  $g_2$  of the anisotropy, are quite sensitive to the input values of the moments.

For the calculation of the theoretical values of the moments with the empirical models of the trace and anisotropy polarizabilities the empirical pair potential BFW and MTT with the parameters in Table 1, was used. Also, the calculations were done using a HFD-B2 potential which is a reference in the literature [65] and the recent ab initio CCSD(T) interatomic potential [91].

The experimentally determined values of the moments, with error limits, now each define a range of acceptable values for the parameters. This approach to the construction of an empirical models for  $\alpha(r)$  and  $\beta(r)$  is acceptable if all moments define a common range of  $g_1$  and  $g_2$ ,  $r_1$  and  $r_2$  values. As we will see below in Tables 4 and 5, the agreement between the experimental values and the theoretical ones using our empirical potential is good and we have verified that it remains acceptable for  $r_1 = 0.486 \pm 0.009 \text{ \AA}$  and  $g_1 = 0.0766 \pm 0.005 \text{ \AA}^3$ , in the case of the trace, and  $r_2 = 0.32 \pm 0.01 \text{ \AA}$  and  $g_2 = 0.14 \pm 0.06 \text{ \AA}^3$ , in the case of the anisotropy models.

## 5. Light scattering induced by collision of two krypton atoms

### 5.1 Experimental and theoretical backgrounds

In this subsection, we simply recall what is collision-induced light scattering (CILS) and its analysis in order to evaluate the polarizability tensor induced by the interactions between two atoms or molecules. Experimentally, by illuminating a gas sample with a laser beam and varying its pressure, it is possible to extract from the scattered light the contribution  $I(\nu)$  due to binary interactions, where  $\nu$  is a frequency shift from the laser beam frequency  $c/\lambda_0$ . This binary intensity  $I(\nu)$  is proportional to the square of the density of the gas [17]. Moreover, by using a polarizer, it is possible to distinguish a “polarized” scattering spectrum  $I_{\perp}(\nu)$  (when the polarization of the incident laser beam is perpendicular to the scattering plane) and a “depolarized” scattering spectrum  $I_{\parallel}(\nu)$  (when this polarization is parallel to the scattering plane). These two intensities are functions of the polarizability tensor of the pair of atoms or molecules considered. More precisely,  $I_{\parallel}(\nu)$  results from the anisotropy  $\beta(r)$  of the tensor while  $I_{\perp}(\nu)$  is generated by both its anisotropy and its trace  $\alpha(r)$ , where  $r$  stands for the interatomic or intermolecular distance. This double dependency can be simply expressed as [1]

$$\begin{pmatrix} I_{\perp}(\nu) \\ I_{\parallel}(\nu) \end{pmatrix} = \begin{pmatrix} 1 & 7/45 \\ 0 & 2/15 \end{pmatrix} \begin{pmatrix} I_0(\nu) \\ I_2(\nu) \end{pmatrix}, \quad (31)$$

Where the intensity  $I_L(\nu)$  is said to be “isotropic” when it is due to the trace ( $L=0$ ) and “anisotropic” when it is due to the anisotropy ( $L=2$ ). Nevertheless, slight numerical corrections must be made to the coefficients involved in Eq.(31) since the experimental collection angle of the scattered light is not exactly zero [92]. In addition, it is usual to plot the depolarized spectrum  $I_{\parallel}(\nu)$  rather than the spectrum  $I_2(\nu)$  to which it is proportional.

Three groups of researchers have published the experimental depolarized binary CILS spectrum of the Krypton atom pair (Proffitt *et al.* [4], Zoppi *et al.*[79] and Dixneuf, Chrysos and Rachet [93]). Their results are very close. Two of these groups (Proffitt *et al.* [4] and Chrysos *et al.* [94]) have

also published the isotropic spectrum, which is much more difficult to obtain. Their results differ significantly. This is partly due to the fact that the measurement uncertainties are very large in this case: the isotropic contribution is obtained from Eq. (31) by the difference  $I_0(\nu) \approx I_{\perp}(\nu) - 7I_{\parallel}(\nu)/6$  even though it is, relatively, a very small contribution at low frequencies. In this work, we privilege the more recent experimental work of the Chryso team (referred to below as DCR). Indeed, the experimental CILS set-up of Angers that this group used allows the detection of very weak signals and has already permit, since its development by Le Duff's group thirty years ago, to detect several isotropic spectra of atomic or molecular pairs.

For a pair of krypton atoms, several models of  $\alpha(r)$  and  $\beta(r)$  can be tested. They can be derived from *ab initio* quantum calculations or from semi-empirical models. In what follows, we consider the two models computed *ab initio* by Maroulis, [84] on the basis of the self-consistent field theory (SCF) and the second-order Møller–Plesset perturbative method (MP2), and the parameterized model (PM) of the trace and the anisotropy described by Eqs. (17-18).

The two polarizability models of Maroulis have been used by DCR in order to reproduce by quantum computational methods the experimental depolarized [93] and isotropic [94] spectra that these authors had measured. Maroulis models can thus serve as a reference for our own calculations of a semi-classical nature, for these two models as well as for the parameterized model defined by Eqs. (17-18).

We have already described in previous papers the semi-classical method we use for the calculation of CILS spectra [95-97]. The intermolecular potential  $V(r)$  being given, we calculate the trajectories of the interacting atoms whether the pair of atoms is in a free state (FR) or in a bound or metastable state (BM) of the effective potential well. For free pairs, using Posch's formulas [98], we compute what are equivalent to Fourier transforms of the trace or anisotropy autocorrelation functions. We then integrate these transforms with respect to the impact parameters and velocities, in the approximation of a Maxwell-Boltzmann velocity distribution. After multiplying by the fourth power of the wave vector  $k_0 = 2\pi/\lambda_0$ , we obtain the contributions of the free pairs to spectral intensities. For the contributions of bound or metastable pairs, we follow the method initiated by Meinander in the anisotropic case [99]. The only difficulty lies in the presence of some Dirac functions which are not eliminated by integration. However, we can replace them by equivalent continuous functions, and this is all the more justified since the input slits of any monochromator used experimentally have a finite width (anyway, because of the presence of the Rayleigh line, it is hardly possible to determine experimentally the CILS intensity in the immediate vicinity of  $\nu=0$ ).

The sum of the two contributions, FR and BM, provides the classical isotropic  $I_0^{cl}(\nu)$  and anisotropic  $I_2^{cl}(\nu)$  intensities. We then check that, for  $n=0, 2$  and  $4$ , the spectral classical moments

$$K_n^{(L)} = 2k_0^{-4} \int_0^{\infty} I_c^{(L)}(\nu) (2\pi\nu)^n d\nu \quad (32)$$

are equal (to within one percent) to the corresponding moments obtained analytically by the sum rule for the corresponding intermolecular potential [100]. We also verify that the proportion of the intensity attributable to bound and metastable dimers is indeed that which can be predicted by Levine's statistical method [101], in both the isotropic and anisotropic cases. For a pair of heavy atoms, this verification is all the more important as the BM contribution is not negligible, at least in the vicinity of the Rayleigh line. For krypton, this proportion is about 20% for the anisotropic spectrum and 10 to 20% for the isotropic spectrum.

Unfortunately, the spectra  $I^c(\nu)$  obtained at this stage are ‘‘classical’’, and thus symmetrical with respect to the Rayleigh line. In order to compare them to the experimental asymmetric spectra, they must be desymmetrized in such a way that the computed asymmetric spectra  $I(\nu)$  respect the detailed balance principle:  $I(\nu)/I(-\nu) = \exp(4\pi\nu\tau_0)$ , where  $\tau_0 = \hbar/2k_B T$ . Thus, it is necessary to use a ‘‘desymmetrization function’’  $D(\nu) = I(\nu)/I^c(\nu)$  such that  $D(-\nu) = \exp(-4\pi\nu\tau_0)D(\nu)$ . We show in Appendix A that this function can be written as  $D(\nu) = (1 + \delta\Lambda(\nu))\exp(2\pi\nu\tau_0)$ , where  $\delta\Lambda(\nu)$  is an even function of quantum origin. In fact, as Frommhold pointed out in his book on collision-induced absorption [102], the different desymmetrization procedures found in the literature lead to substantially different semiclassical spectral profiles. In previous papers [96, 97], we proposed to fit a linear combination of the three most commonly used desymmetrization functions  $\exp(2\pi\nu\tau_0)/\cosh(2\pi\nu\tau_0)$ ,  $2\pi\nu\tau_0 \exp(2\pi\nu\tau_0)/\sinh(2\pi\nu\tau_0)$  and  $\exp(2\pi\nu\tau_0)$ . The coefficients  $\varphi_0$ ,  $\varphi_1$  and  $\varphi_2$  of this combination were adjusted so that the spectral moments  $M_0$ ,  $M_1$  and  $M_2$  of the semiclassical spectrum are equal to those deduced from the classical moments  $K_0$ ,  $K_2$  and  $K_4$  and their Wigner-Kirkwood (WK) quantum corrections  $\delta K_{2n}$  obtained by the sum rule. Here we used a method giving similar results, but on a more theoretical basis, by directly deducting an approximate expansion of  $\delta\Lambda(\nu)$  up to  $\nu^4$  from the values of  $\delta K_0$ ,  $\delta K_2$  and  $\delta K_4$ . This new method is presented in Appendix A. In the studied case of krypton, it results in a desymmetrization function close to  $\exp(2\pi\nu\tau_0)$ , generally taking very slightly lower values at low frequencies (by a few %) and slightly higher at higher frequencies (by a few %).

## 5.2. Results and discussion

The objective of this work was to test our empirical models of trace and anisotropy of polarizability, defined by equations (17-18) and Table 3, and to evaluate the influence of available

intermolecular potentials of Krypton on the computed isotropic and depolarized spectra. In order to do so, we considered four potential models: the “old” HFD-B2 potential of Aziz and co-workers [65], a “CCSD” potential recently computed by Fakhardji *et al.* at the CCSD(T) level with an aug-cc-pV5Z basis set, including relativistic effects (ECP10MDF) of the inner core electrons, [91] and the two potentials MTT and BFW described above.

#### *a) Depolarized spectrum*

First, we tested our semi-classical calculations by comparing the depolarized spectra obtained for the SCF and MP2 anisotropies of the interaction polarizability of two Kr Atoms calculated by Maroulis [84] and the HFD-B2 potential with the corresponding computed spectra obtained by DCR [93] using quantum means. For the SCF and MP2 anisotropies, we find within a few percent the intensities calculated by DCR over the whole width (from 0 to 140  $\text{cm}^{-1}$ ) of the experimental spectrum: our depolarized spectral profiles and those of DCR are difficult to distinguish on a logarithmic scale. This confirms in our opinion the relevance of our semiclassical calculations for the pair of relatively heavy atoms that are those of Krypton and in the limited frequency domain that is that of the available experimental measurements.

Next, we calculated the depolarized spectra for each of the above mentioned potentials and for three polarizability models: SCF and MP2 of Maroulis and the parameterized one (PM) described by Eq. (18). The results are summarized in Table 4 and in figures 2 to 5. Table 4 and Fig. 2 allow the reader to compare the spectral moments that can be deduced from experimental DCR measurements and those that can be deduced from the different calculated spectra. The three figures 3 to 5 show the depolarized (anisotropic) spectra: experimental (DCR) and calculated for each of the three polarization models (each time for the four selected potentials).

Table 4 shows the values of the moments  $M_n$  ( $n=0$  to 4) calculated for each of the four potentials and the three anisotropy models against the corresponding values we were able to deduce from the experimental DCR spectrum [93]. The latter starts only at 4  $\text{cm}^{-1}$ . However, we could see that, whatever the anisotropy and potential models used in this work, the fractions of moments attributable to the interval  $[-4, 4] \text{ cm}^{-1}$  are systematically 42% for  $M_0$ , 2% for  $M_1$  and  $M_2$ , 0.02% for  $M_3$  and  $M_4$ . We were thus able to deduce the values of the experimental moments from the portions of moments attributable to the intervals  $[4, 135] \text{ cm}^{-1}$  (measured experimentally) and  $[135, \infty[ \text{ cm}^{-1}$  (extrapolated thanks to a decreasing exponential function). In the table, we also give the minimum and maximum values of these experimental moments, considering the uncertainty bars provided by DCR.

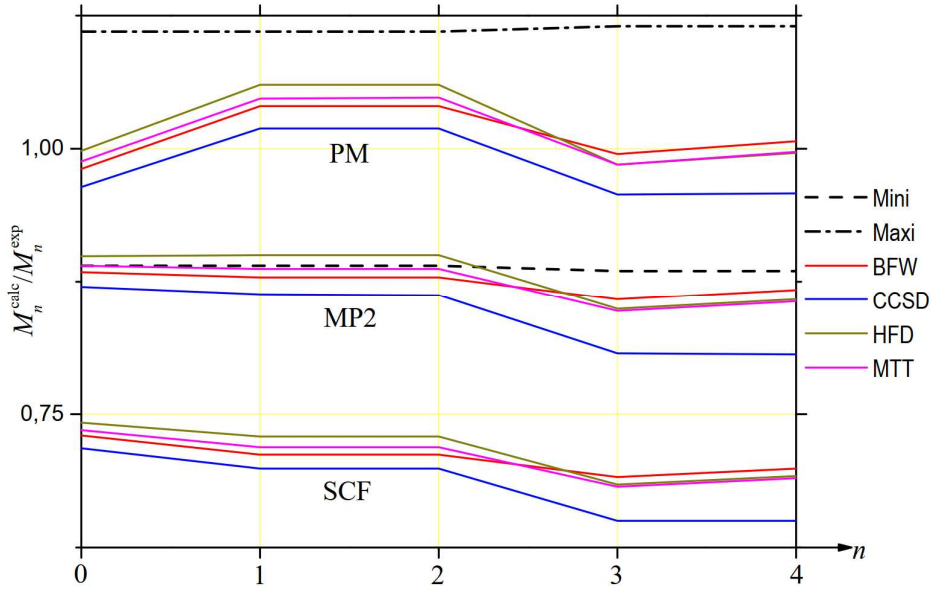
**Table 4.** : Experimental and calculated spectral moments of the depolarized CILS spectrum of krypton. The experimental moments are extrapolated from the experimental spectrum published by DCR [93].

	Mini	Experiment	Maxi		PM/BFW	PM/CCSD	PM/HFD	PM/MTT	units
$M_0$	197.3	221.6	246.0		217.47	213.59	221.29	218.98	$\text{\AA}^9$
$M_1$	0.920	1.036	1.151		1.079	1.056	1.099	1.087	$10^{13} \text{\AA}^9 \text{s}^{-1}$
$M_2$	7.136	8.020	8.905		8.349	8.169	8.508	8.410	$10^{26} \text{\AA}^9 \text{s}^{-2}$
$M_3$	3.291	3.717	4.142		3.763	3.555	3.726	3.727	$10^{38} \text{\AA}^9 \text{s}^{-3}$
$M_4$	2.567	2.899	3.232		2.925	2.778	2.894	2.896	$10^{52} \text{\AA}^9 \text{s}^{-4}$

	SCF/BFW	SCF/CCSD	SCF/HFD	SCF/MTT	MP2/BFW	MP2/CCSD	MP2/HFD	MP2/MTT	units
$M_0$	161.92	159.23	164.57	162.98	196.09	192.79	199.37	197.40	$\text{\AA}^9$
$M_1$	0.7388	0.7243	0.7564	0.7457	0.9117	0.8937	0.9334	0.9203	$10^{13} \text{\AA}^9 \text{s}^{-1}$
$M_2$	5.718	5.605	5.854	5.771	7.056	6.916	7.224	7.122	$10^{26} \text{\AA}^9 \text{s}^{-2}$
$M_3$	2.620	2.417	2.593	2.586	3.248	3.000	3.222	3.207	$10^{38} \text{\AA}^9 \text{s}^{-3}$
$M_4$	2.042	1.886	2.02	2.014	2.527	2.338	2.513	2.494	$10^{52} \text{\AA}^9 \text{s}^{-4}$

Figure 2 allows a more immediate comparison between the experimental and calculated moments. For each of the twelve calculated spectra (four potentials and three anisotropies), the moments are divided by the corresponding experimental moments.



**Fig. 2.** Evolution of the ratio  $M_n^{\text{calc}}/M_n^{\text{exp}}$  of calculated to experimental depolarized moments when  $n$  varies from 1 to 4. Three anisotropy models (PM, MP2 and SCF [84]) and four intermolecular potential models (BFW in red, CCSD in blue, HFD in brown, MTT in indigo) are considered. Due to experimental uncertainties reported by DCR [93], the values of these ratios must be contained in the vicinity of one between the two black curves (dash and dash-dot).

Only the parameterized model (PM) provides moment ratios close to one and in the range determined by the uncertainty bars. The moments associated with the MP2 model and especially SCF are too low, as expected. In their paper [93], DCR had already noted the insufficient spectral intensities of these two models provided by Maroulis with respect to their own experimental measurements. In the case of the SCF model, the lack of intensity is accentuated by not taking into account the dynamic electron correlation effects. The influence of the potential on the values of the



moments can also be appreciated from figure 2. The “old” HFD-B2 potential of Aziz *et al.* [65] is the one that generates the largest values of  $M_0$  (low frequencies),  $M_1$  and  $M_2$  (medium frequencies) while the largest values of  $M_3$  and  $M_4$  (high frequencies) are generated by the BFW potential. The recent CCSD potential [91] is the one that consistently generates the lowest moments. In view of the experimental uncertainties, it is difficult to decide between the different potentials. Nevertheless, we note that the BFW potential is the one for which the deviation of the calculated moments from the successive experimental moments undergoes the least relative variations.

Unfortunately, the analysis of  $M_n$  moments is not sufficient because it is increasingly uncertain as  $n$  grows. Figures 3 to 5 provide further evidence. Concerning the potentials, the MTT potential and especially the BFW potential systematically produce slightly higher intensities than the HFD-B2 potential at higher frequencies (beyond  $90\text{ cm}^{-1}$ ). Conversely, the CCSD potential generally produces slightly lower intensities. Nevertheless, these potentials produce similar and even very similar intensities at the lowest frequencies. Due to its error bars, the CIS experimental spectra cannot really discriminate between them. Figures 3 and 4 confirm what had already been observed by DCR: the SCF model and to a lesser extent the MP2 model generate lower intensities than those measured experimentally. In the case of the MP2 model, one can nevertheless notice that, if it seems to underestimate the absolute intensities as they were measured (from 16% at  $70\text{ cm}^{-1}$  to 38% at  $135\text{ cm}^{-1}$ ), it reproduces rather well the general profile of the scattered spectrum. Unfortunately, this is not always the case for the parameterized model (PM), even though this model is the one that the analysis of spectral moments gives as the best. The agreement with the experimental results is almost perfect up to  $90\text{ cm}^{-1}$ : the calculated curve falls within all the experimental uncertainty bars, whatever the potential considered. Beyond  $100\text{ cm}^{-1}$ , however, it deviates significantly (the BFW potential being the one that deviates the least). While the experimental curve continues to present a positive concavity, the calculated curve adopts a negative concavity. Moreover, the latter appears to be more sensitive to the potential used. In fact, this PM curve presents a secondary minimum around  $160\text{ cm}^{-1}$  (depending on the chosen potential) followed by a secondary maximum 20 to  $30\text{ cm}^{-1}$  further (this rebound explains why the values of  $M_3$  and  $M_4$  are not penalized by the drop in intensity that precedes it). In our opinion, this type of behavior is associated with the exponential damping term present in Eq. (18): it is such that the derivative of the anisotropy cancels at  $3.20\text{ \AA}$  (short range effects, below the intermolecular diameter of about  $3.6\text{ \AA}$ ) and becomes negative below (which is not the case for the SCF and MP2 models). This kind of disagreement shows the difficulty of fitting an empirical curve that accounts for both low and high frequency spectral intensities. But it confirms in any case the interest of obtaining experimental spectra in wide frequency ranges.

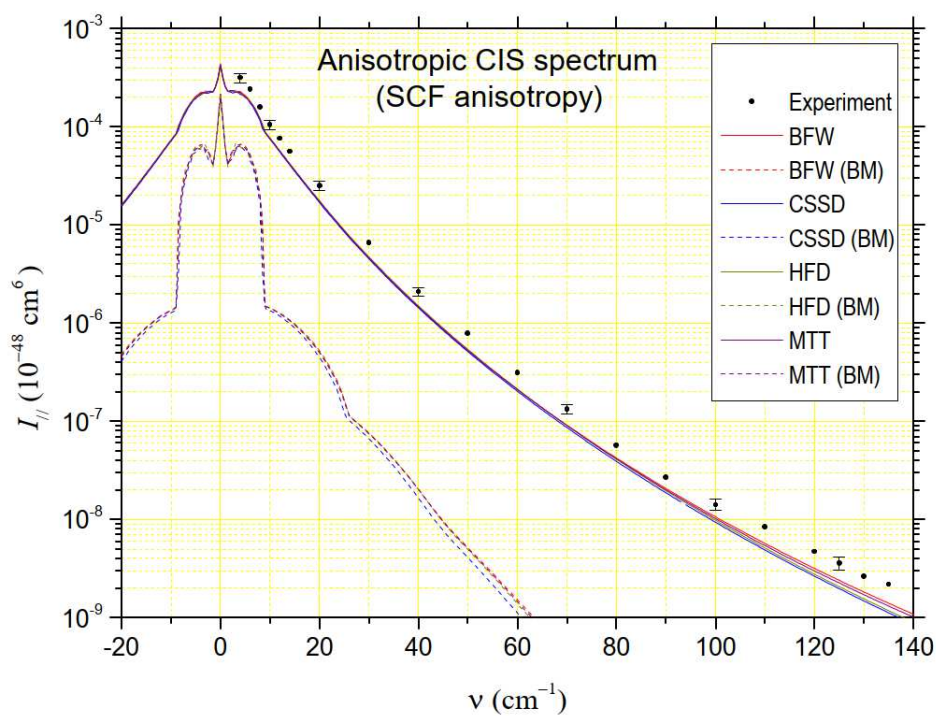


**Fig. 3.** Comparison between the calculated depolarized CILS spectra of  $\text{Kr}_2$  at  $T=294.5$  K using different interatomic potentials (BFW: red; CCSD: blue; HFD-B: brown; MTT: indigo) and *ab initio* SCF pair polarizability anisotropy of Maroulis [84] with the experimental measurements. The bound and metastable pair contributions are represented by dashed lines.

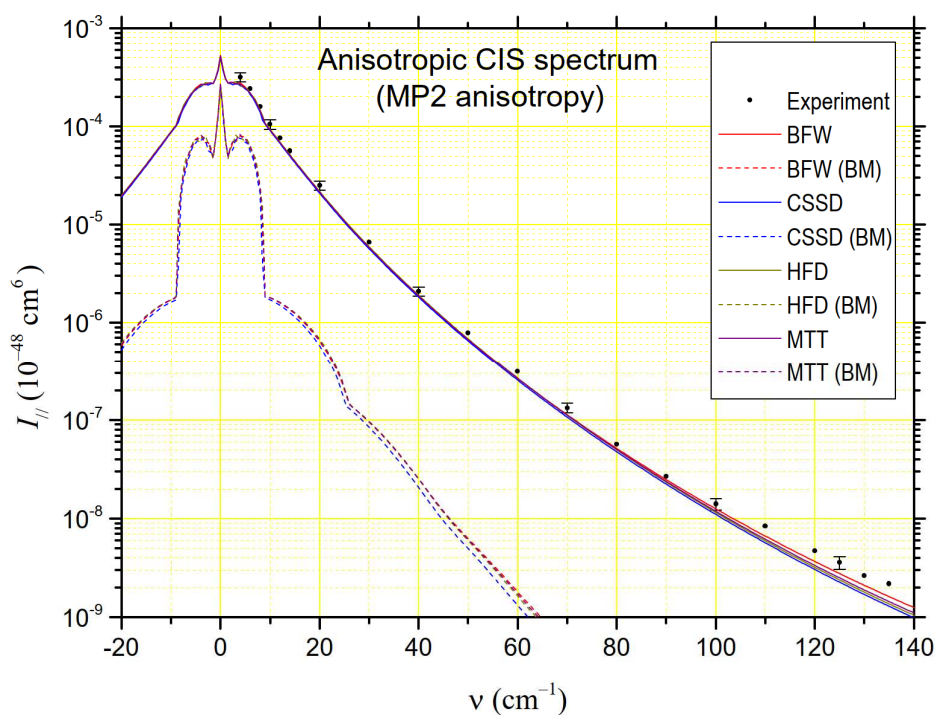


**Fig. 4.** The same comparison as in Figure 3 between depolarized spectra generated by four potentials but for the MP2 pair polarizability anisotropy of Maroulis [84].

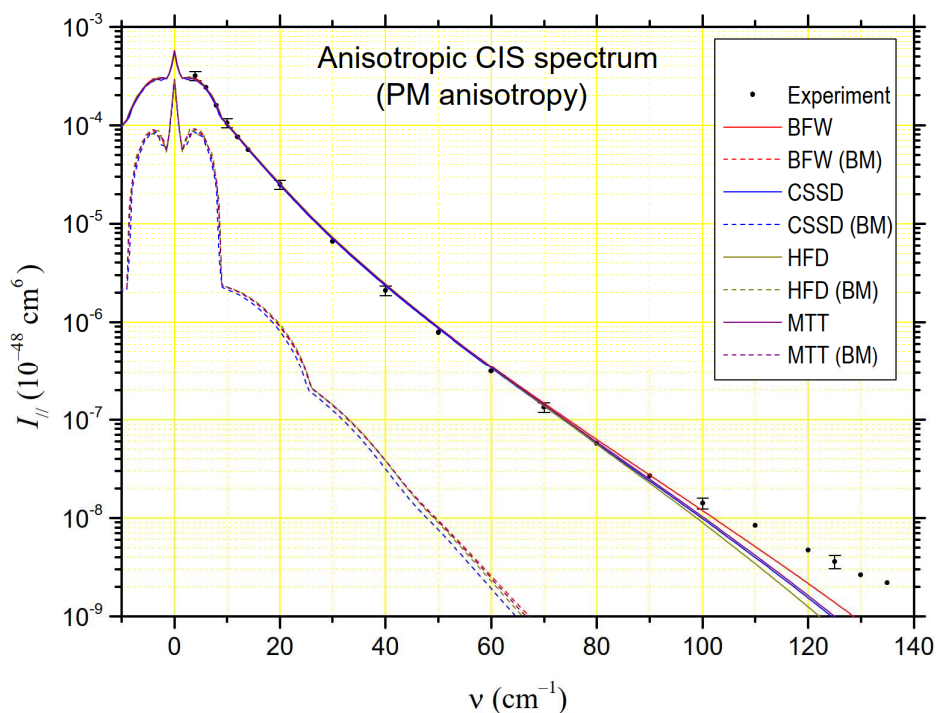


**Fig. 5.** The same comparison as in Figure 3 between depolarized spectra generated by four potentials but for the PM pair polarizability anisotropy defined by Eq. (18).

#### b) Isotropic spectrum

The difficulties encountered in the depolarized spectrum are even greater in the case of the isotropic spectrum. Because of much lower intensities at low frequencies and the large uncertainties that necessarily accompany the evaluation of such a spectrum (from the difference between two quantities of similar amplitudes), the experimental spectrum cannot really constitute a reliable basis for discriminating between the PM, MP2 and SCF models. Besides, the frequency range explored experimentally by Chrysos and Rachet [94], from 80 to 135  $\text{cm}^{-1}$ , is responsible for only a small fraction of the successive spectral moments. Moreover, unlike what can be seen in the anisotropic case, the fractions attributable to the [80, 135]  $\text{cm}^{-1}$  interval diverge in a non-negligible way depending on the anisotropy model used in the calculations; in particular, the SCF model differs clearly from the other two. For PM and MP2, we found that the interval [80, 135]  $\text{cm}^{-1}$  contributes  $\approx 3.4\%$  of the moment  $M_0$  (SCF: 2.4%),  $\approx 27\%$  of  $M_1$  and  $M_2$  (SCF: 20%) and  $\approx 62\%$  of  $M_3$  and  $M_4$  (SCF: 54%). The values of the experimental moments reported in Table 5 are extrapolated from the averages between MP2 and PM and the four potentials considered. In any case, the experimental uncertainties are so large (between +150% and -60% at 100  $\text{cm}^{-1}$ ) that the reported moments can only be considered as orders of magnitude rather than measurements.

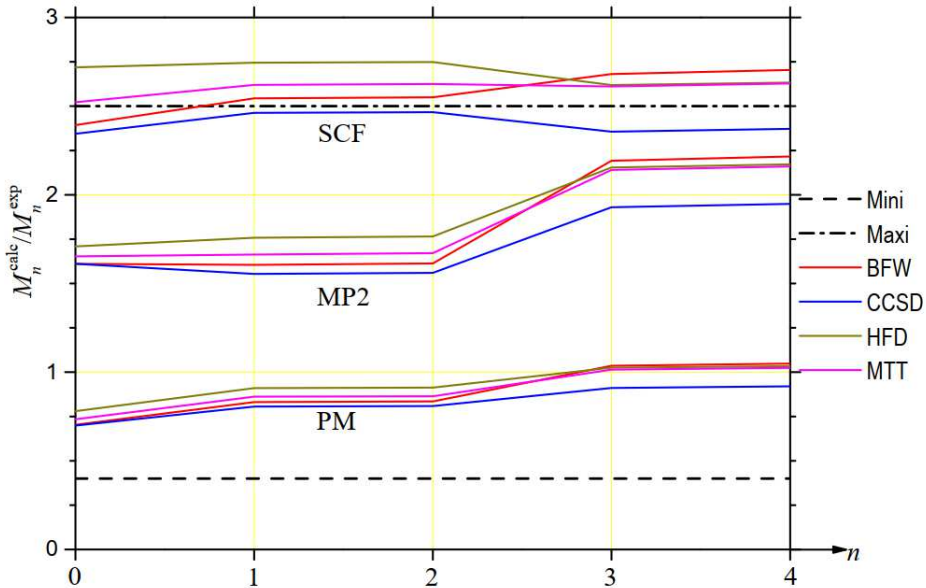
**Table 5.** Experimental and calculated spectral moments of the isotropic CILS spectrum of krypton. The experimental moments are extrapolated from the experimental spectrum published in [94]. Since the latter starts only at  $80 \text{ cm}^{-1}$ , the portions of moments attributed to  $[-80, 80] \text{ cm}^{-1}$  are those that can be roughly deduced from the calculated spectra.

	Mini	Experiment	Maxi		PM/BFW	PM/CCSD	PM/HFD	PM/MTT	units
$M_0$	1.09	2.72	6.80		1.72	1.71	1.91	1.80	$10^{-2} \text{ \AA}^9$
$M_1$	0.57	1.42	3.55		1.07	1.04	1.18	1.11	$10^{10} \text{ \AA}^9 \text{ s}^{-1}$
$M_2$	0.44	1.10	2.76		0.84	0.81	0.92	0.87	$10^{24} \text{ \AA}^9 \text{ s}^{-2}$
$M_3$	0.84	2.11	5.27		2.09	1.83	2.06	2.04	$10^{36} \text{ \AA}^9 \text{ s}^{-3}$
$M_4$	0.66	1.65	4.12		1.65	1.45	1.63	1.61	$10^{50} \text{ \AA}^9 \text{ s}^{-4}$

	SCF/BFW	SCF/CCSD	SCF/HFD	SCF/MTT	MP2/BFW	MP2/CCSD	MP2/HFD	MP2/MTT	units
$M_0$	5.85	5.73	6.65	6.17	3.94	3.94	4.18	4.04	$10^{-2} \text{ \AA}^9$
$M_1$	3.29	3.18	3.55	3.38	2.07	2.00	2.27	2.15	$10^{13} \text{ \AA}^9 \text{ s}^{-1}$
$M_2$	2.56	2.48	2.76	2.63	1.62	1.57	1.77	1.68	$10^{26} \text{ \AA}^9 \text{ s}^{-2}$
$M_3$	5.40	4.74	5.27	5.25	4.41	3.89	4.34	4.31	$10^{38} \text{ \AA}^9 \text{ s}^{-3}$
$M_4$	4.26	3.74	4.15	4.14	3.49	3.07	3.42	3.40	$10^{52} \text{ \AA}^9 \text{ s}^{-4}$

As can be seen in Figure 6, the model closest to these evaluations remains the parameterized model (PM) for which the  $M_n^{\text{cal}}/M_n^{\text{exp}}$  ratios are closest to one. The SCF model is the furthest from this value, as in the anisotropic case, approaching or exceeding the upper limit of the experimental moments.



**Fig. 6.** Evolution of the ratio  $M_n^{\text{cal}}/M_n^{\text{exp}}$  of calculated to experimental isotropic moments when  $n$  varies from 1 to 4. Three trace models (MP, MP2 and SCF [84]) and four intermolecular potential models (BFW in red, CCSD in blue, HFD in brown, MTT in indigo) are considered. Due to experimental uncertainties reported in [94], the values of these ratios must be contained between the two black curves (dash and dash-dot).

Curiously, while the increasing order of the depolarized moment intensities is SCF-MP2-PM, it is exactly the reverse order that is displayed in Fig. 6. The same observation can be deduced from

the comparison of figures 7 to 9. The two Maroulis models, SCF in particular, generate higher intensities than those measured, while the parameterized model (PM) produces generally lower intensities. All three models remain consistent with the measurements due to the large uncertainty bars. Nevertheless, none of the three models sufficiently reproduces at the highest frequencies the strong negative concavity of the experimental curve, either due to experimental uncertainty or associated with short-range effects in the vicinity of the potential wall. We certainly noted that the curves generated by each of the three models also curved quite strongly beyond  $250\text{ cm}^{-1}$ , presenting a minimum and then a secondary maximum, but at much higher frequencies and depending strongly on the potential used. This leads us to think that the three trace models must be described more finely at very short distances, below the molecular diameter.

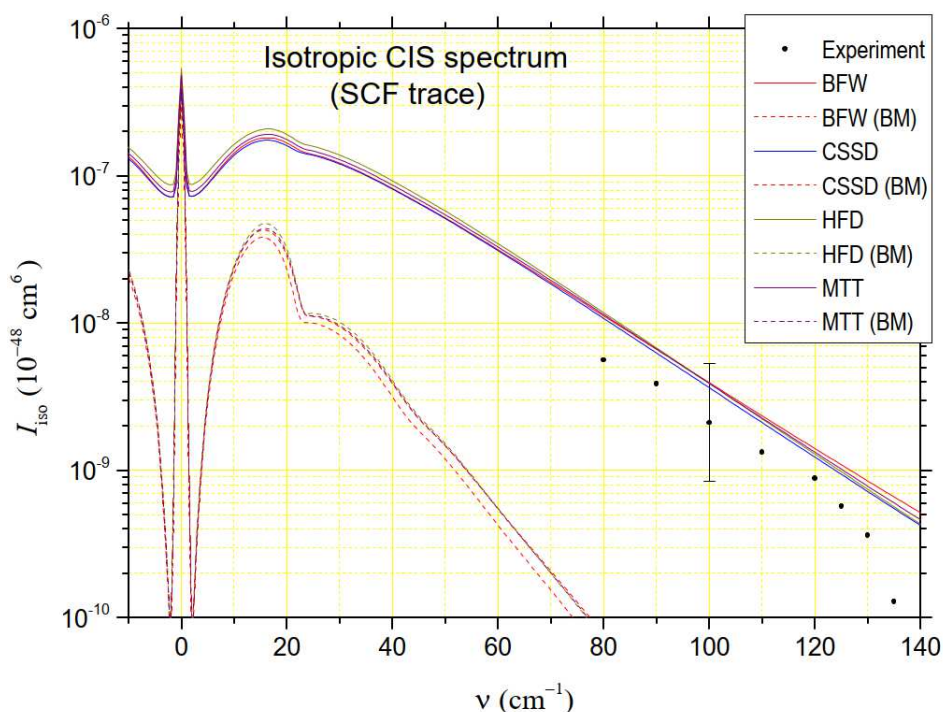


**Fig. 7.** Comparison between the calculated isotropic CILS spectra of  $\text{Kr}_2$  at  $T=294.5\text{ K}$  using different interatomic potentials (BFW: red; CCSD: blue; HFD-B: brown; MTT: indigo) and *ab initio* SCF pair polarizability trace of Maroulis [84] with the experimental measurements. The bound and metastable pair contributions are represented by dashed lines.

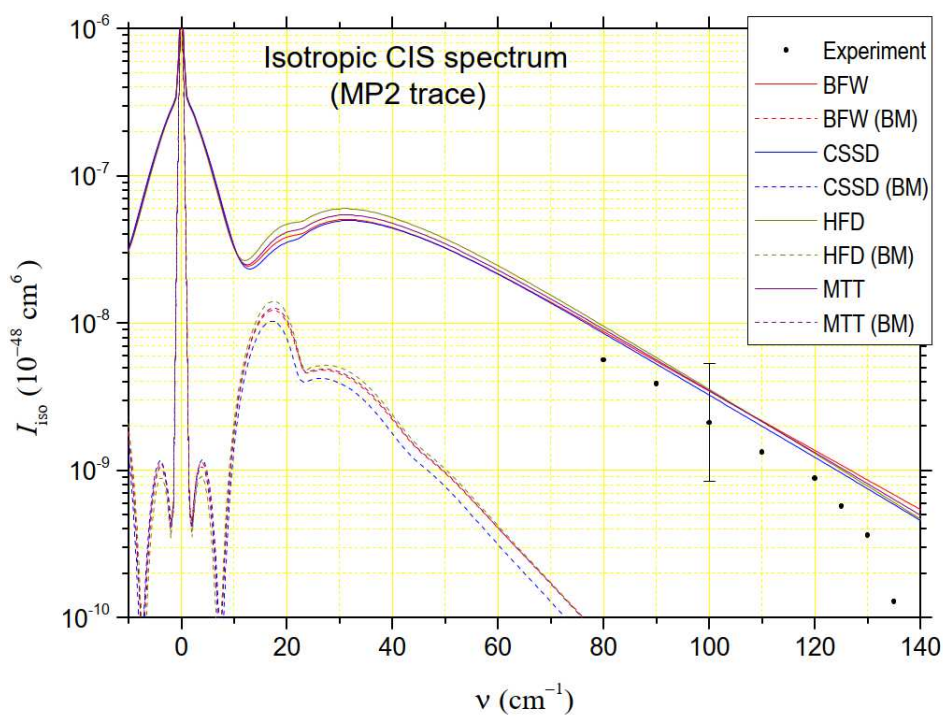


**Fig. 8.** The same comparison as in Figure 7 between isotropic spectra generated by four potentials but for the MP2 pair polarizability trace of Maroulis [84].

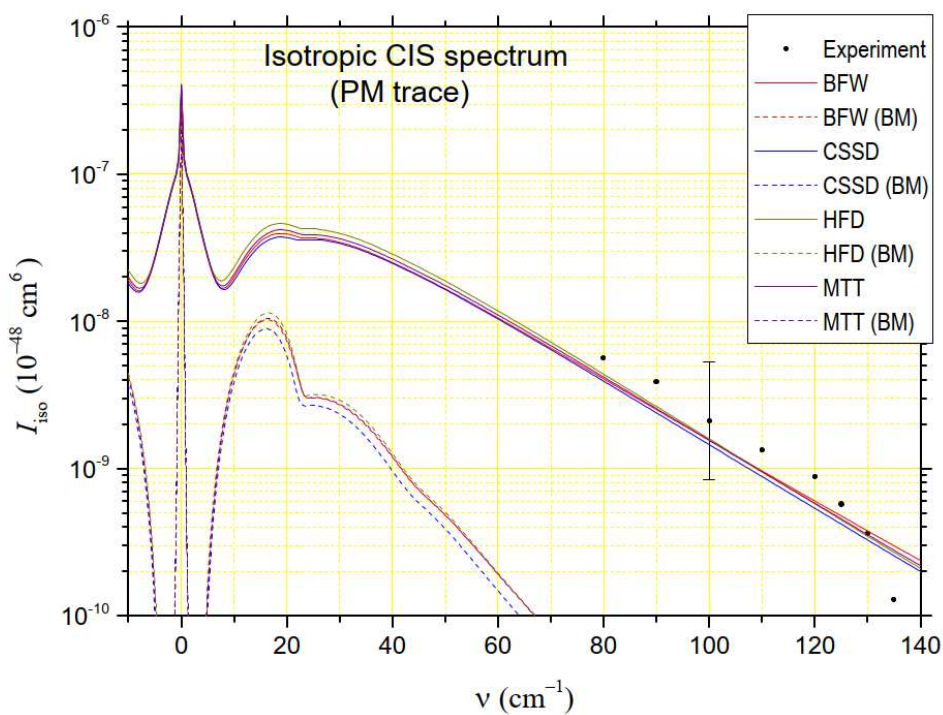


**Fig. 9.** The same comparison as in Figure 7 between isotropic spectra generated by four potentials but for the PM pair polarizability trace defined by Eq. (17).

## 5. Conclusion

The empirical krypton potentials presented in this work, MTT and especially BFW, as well as the parameterized anisotropy model of krypton pair polarizability, provide the best agreement between the experimental krypton light scattering spectrum measured by Dixneuf-Chrysos-Rachet [93] and the numerical calculation, both for the first  $M_n$  spectral moments ( $n=0$  to 4) and for the spectral line shape. However, the agreement is less good at higher frequencies with respect to the parameterized anisotropy model. Beyond the experimental uncertainties which can partly explain such a disagreement, this one underlines the need to refine the models at very short distances, in the vicinity of the potential wall, and to minimize the effect of the propagation of numerical uncertainties in the numerical calculations at high frequencies (this numerical problem has been studied for quantum approaches but, to our knowledge, not in such a thorough manner in the semiclassical case [103-105]). As for the depolarized spectrum, we also evaluated the spectral moments of the isotropic spectrum of krypton measured by Chrysos-Rachet [94] from a comparison of the experimental data with our theoretical spectra. Nevertheless, the narrowness (due to the fact that the isotropic spectrum cannot be measured directly but by subtracting two spectra of similar intensities) of the frequency interval explored as well as the amplitude of the experimental uncertainties prevent to discriminate between the trace models used in this work (MP2 and SCF of Maroulis [84] and parameterized model). Here again, the values taken by the trace at short distances appear to be decisive at high frequencies. In summary, however, we obtain good overall agreement between experimental measurements and calculations based on the combined use of parameterized models of the pair polarizability and the BFW interatomic potential of krypton, which in our opinion grounds the interest of the method we have developed.

## Acknowledgments

We are very grateful to F. Rachet for sending us his experimental data of the isotropic spectrum of krypton.

## APPENDIX A: New determination of a desymmetrization function

As defined in Eq.(32), the successive classical moments  $K_{2n}^{(L)}$  can be computed from the computed classical spectrum  $I_c^{(L)}(\nu)$  (with  $L=0$  for the trace and  $L=2$  for the anisotropy of the polarizability tensor). If the calculation of this spectrum is well done, the moments  $K_0$ ,  $K_2$  and  $K_4$  should be equal to the corresponding values obtained by the sum rule. The hypothetical desymmetrization function  $D(\nu)=I^{(L)}(\nu)/I_c^{(L)}(\nu)$  transforms this symmetric spectrum into a dissymmetric  $I^{(L)}(\nu)$  respecting the detailed balance principle:  $I^{(L)}(\nu)=\exp(4\pi\nu\tau_0)I^{(L)}(-\nu)$ , where  $\tau_0=\hbar/2k_B T$ . By positing  $D(\nu)=\exp(2\pi\nu\tau_0)(1+\delta\Lambda(\nu))$ , the function to determine becomes an even function  $\delta\Lambda(\nu)$ . This function of quantum origin must be equal to zero at the classical limit  $\tau_0=0$  and thus is proportional to a positive power of  $\tau_0$ . We will see later that this function must be proportional to  $\tau_0^2$ . Under these conditions, the spectral moments of even or odd order

$$M_n^{(L)} = k_0^{-4} \int_{-\infty}^{\infty} D(\nu) I_c^{(L)}(\nu) (2\pi\nu)^n d\nu \quad (\text{A1})$$

can be expressed as:

$$\begin{cases} M_{2n}^{(L)} = 2k_0^{-4} \int_0^{\infty} \cosh(2\pi\nu\tau_0) (1+\delta\Lambda(\nu)) I_c^{(L)}(\nu) (2\pi\nu)^{2n} d\nu \\ M_{2n+1}^{(L)} = 2k_0^{-4} \int_0^{\infty} \sinh(2\pi\nu\tau_0) (1+\delta\Lambda(\nu)) I_c^{(L)}(\nu) (2\pi\nu)^{2n+1} d\nu \end{cases} \quad (\text{A2})$$

At the classical limit,  $\cosh(2\pi\nu\tau_0)(1+\delta\Lambda(\nu))=1$  and  $M_{2n}^{(L)}=K_{2n}^{(L)}$ , whereas  $\sinh(2\pi\nu\tau_0)=0$  and  $M_{2n+1}^{(L)}=0$ . Besides, the radii of convergence of the expansions of  $\cosh(x)$  and  $\sinh(x)$  being infinite, we can use these expansions inside the integrals of Eqs.(A2). For a given value of  $L$ ,

$$\begin{cases} M_{2n} = \sum_{p=0}^{\infty} \frac{\tau_0^{2p}}{(2p)!} K_{2(p+n)} + \delta K_{2n} \\ \frac{M_{2n+1}}{\tau_0} = \sum_{p=0}^{\infty} \frac{\tau_0^{2p}}{(2p+1)!} K_{2(p+n+1)} + \frac{\delta K_{2n+1}}{\tau_0} \end{cases} \quad (\text{A3})$$

where

$$\begin{cases} \delta K_{2n} = 2k_0^{-4} \int_0^{\infty} \cosh(2\pi\nu\tau_0) \delta\Lambda(\nu) I_c(\nu) (2\pi\nu)^{2n} d\nu \\ \delta K_{2n+1} = 2k_0^{-4} \int_0^{\infty} \sinh(2\pi\nu\tau_0) \delta\Lambda(\nu) I_c(\nu) (2\pi\nu)^{2n+1} d\nu \end{cases} \quad (\text{A4})$$



are quantum corrections specifically related to the system studied. By combining the equations of (A3), since  $1/(2p+1)! = 1/(2p)! - 2p/(2p+1)!$ , we get also:

$$\frac{M_{2n+1}}{\tau_0} = M_{2n+2} - \sum_{p=1}^{\infty} \frac{2p \tau_0^{2p}}{(2p+1)!} K_{2(p+n+1)} + \frac{\delta K_{2n+1}}{\tau_0} - \delta K_{2n+2} \quad (\text{A5})$$

Therefore, up to the second-order in power of  $\tau_0$  (which eliminates the subtraction  $\delta K_{2n+1}/\tau_0 - \delta K_{2n+2}$ ):

$$\left\{ \begin{array}{l} M_{2n} = K_{2n} + \delta K_{2n} + \frac{\tau_0^2}{2} K_{2n+2} \\ \frac{M_{2n+1}}{\tau_0} = K_{2n+2} + \delta K_{2n+2} + \frac{\tau_0^2}{6} K_{2n+4} \\ \phantom{\frac{M_{2n+1}}{\tau_0}} = M_{2n+2} - \frac{\tau_0^2}{3} K_{2n+4} \end{array} \right. \quad (\text{A6})$$

At order two in  $\tau_0$ , the semiclassical spectral moments can be expressed in terms of the classical  $K_{2n}$  spectral moments, the dynamical quantum corrections in  $\tau_0^2 K_{2n}$ , and the specific quantum corrections  $\delta K_{2n}$ .<sup>1</sup> These three contributions can also be computed by using the sum rule. Expressions for the  $K_{2n}$  moments are given for example in [100] for  $2n=0, 2$  and  $4$  using the classical pair correlation function  $g(r) = \exp(-V(r)/k_B T)$ , where  $V(r)$  is the value of the intermolecular potential at distance  $r$  (considered as isotropic in first approximation). The 2<sup>nd</sup>-order in  $\tau_0$  Wigner-Kirkwood (WK) expansion of the pair correlation function in the case of an isotropic potential [106],

$$\delta g(r) = \frac{\tau_0^2}{3m} \left( \frac{1}{2k_B T} \left( \frac{dV(r)}{dr} \right)^2 - \frac{2}{r} \frac{dV(r)}{dr} - \frac{d^2 V(r)}{dr^2} \right) g(r), \quad (\text{A7})$$

where  $m$  is the reduced mass of the molecular pair, does not intervene in the writing of these classical  $K_{2n}$  moments. Conversely, we assume that this WK expansion generates the  $\delta K_{2n}$  corrections defined by Eq. (A4). To obtain them, we simply replace the classical pair correlation function  $g(r)$  with the corrective  $\delta g(r)$  in the sum rule expressions of the  $K_{2n}$  moments. As long as corrections in power of  $\tau_0$  limited to order 2 remain valid, the values of  $\delta K_0$ ,  $\delta K_2$  and  $\delta K_4$  defined by Eq. (A4a) can be posited equal to the WK corrections of the moments  $K_0$ ,  $K_2$ , and  $K_4$ , respectively. Moreover, in accordance with the initial assumptions on the even-function  $\delta \Lambda(v)$ , the

---

<sup>1</sup> This expansion shows that dynamical corrections must be taken into account even for  $M_0$  contrary to what was asserted by Hartye *et al.* [106] and taken up by Frommhold [102] and ourselves in a previous paper [97]. However, this dynamical correction of  $M_0$  is very small, at least in the case of Krypton (less than one per thousand). The relative importance of dynamical corrections increases with the order  $n$ .

latter and the integrals  $\delta K_{2n}$  are proportional to  $\tau_0^2$  (the  $\delta$ -symbol used here implies proportionality to  $\tau_0^2$ ). Since the  $K_6$  moment can be deduced from the computed classical spectrum,<sup>2</sup> we obtain from Eqs.(A6) and the WK corrections the values of the five first spectral moments  $M_0, M_1, M_2, M_3$  and  $M_4$ . Moreover, we can make an approximation of the even function  $\delta\Lambda(\nu)$  up to order 4 in power of  $\nu$ . By positing  $\delta\Lambda(\nu) \approx \tau_0^2(\varphi_0 + \varphi_1\nu^2 + \varphi_2\nu^4)$  within Eq. (A4a), for  $2n=0, 2$  and  $4$ , we obtain a system of 3 equations involving  $\delta K_0, \delta K_2$ , and  $\delta K_4$  with 3 unknowns ( $\varphi_i$ ) that is simple to solve and can be considered as valid for the limited frequency domain of the study (of course, this limited development ceases to be valid at higher frequencies). The spectral intensity  $I^{(L)}(\nu) = I_c^{(L)}(\nu) \exp(2\pi\nu\tau_0)(1 + \delta\Lambda(\nu))$  is then completely determined within the approximations used.

---

<sup>2</sup> An analytical expression for the  $K_6$  moment of the anisotropic spectrum has been published in Ref. [107] and reproduced recently in Ref. [81]. Unfortunately, one term of this complex expression does not have the physical dimension of the other terms, which makes it questionable. Even if it is numerically more inaccurate, it is simpler to use the value of  $K_6$  calculated from the classical depolarized spectrum, especially in the Krypton case since the uncertainty on this value has a small impact on the value of  $M_4$  (the corresponding dynamical correction is then of the order of 1.5%; the uncertainty on it is a priori negligible).

## References

---

1. Frommhold L, Adv. Chem. Phys. 1981; **46**: 1.
2. Tabisz GC, Mol. Spectrosc. 1979; **6**: 136.
3. Gelbart WM, Adv. Chem. Phys. 1974; **26**: 1.
4. Proffitt MH, Keto JW, Frommhold L., 1981; Can. J. Phys. **59**: 1459.
5. El-Kader MSA, Godet J-L , Gustafsson M, Maroulis G, J. of Quant. Spectr. & Rad. Transf. 2018; **209**: 232.
6. El-Kader MSA, Mostafa SI, Bancewicz T, Maroulis G, Chem. Phys. 2014; **440**: 127.
7. El-Kader MSA, El-Sheikh SM, Bancewicz T, Hellmann R, J. Chem. Phys. 2009; **131**: 044314.
8. El-Kader MSA, Mol. Phys. 2013; **111**: 307.
9. El-Kader MSA, El-Eraky SM., Z. Phys. Chem. 2005; **219**: 181.
10. El-Kader MSA, Mol. Phys. 2011; **109**: 863.
11. El-Kader MSA, Z. Phys. Chem. 2005; **219**: 1169.
12. El-Kader MSA, Chem. Phys. 2008; **352**: 311.
13. El-Kader MSA, Godet J-L, El-Sadek AA, Maroulis G, Mol. Phys. 2017; **115**: 2614
14. El-Kader MSA, Phys. Lett. A, 2009; **373**: 2054.
15. El-Kader MSA, Bancewicz T, Mol. Phys. 2011; **109**: 457.
16. Ulivi L, Meinander N, Barocchi F, Phys. Rev. Lett. 1995; **75**: 3094.
17. ElliasmineA, Godet J-L, Le Duff Y, Mol. Phys. 1997; **90**: 147.
18. Cohen ER, Birnbaum G, J. Chem. Phys. 1975; **62**: 3807.
19. Maitland GC, Rigby M, Smith EB, Wakeham WA, Intermolecular Forces – Their Origin and Determination, Clarendon, Oxford 1981. Doi: 10.1002/bbpc.19830870335
20. Maitland GC, Wakeham WA, Mol. Phys. 1978; **35**: 1443.
21. Dymond JH, Marsh KN, Wilhoit RC, Wong KC, Virial coefficients of pure gases and mixtures, edited by Frenkel M and Marsh KN, Landolt-Bornstein - Group IV Physical Chemistry, 21, Subvolume A “Virial coefficients of Pure Gases”, Springer-Verlag, Heidelberg 2002.
22. Fender BEF, Halsey GD Jr., J. Chem. Phys. 1962; **36**: 1881.
23. Weir RD, Wynne-Jones WFK, Rowlinson J S, Saville G, Trans. Faraday Soc. 1967; **63**: 1320.
24. Byrne MA, Jones MR, Staveley LAK, Trans. Faraday Soc. 1968; **64**: 1747.
25. Thomaes G, Van Steenwinkel R, Nature (London) 1962; **193**: 160.
26. Brewer J, Air Force Off. Sci. Res.,[Tech. Rep.] AFOSR-TR 67-2795, 1967.
27. Pollard CA, Ph.D. Thesis, Univ. London, England 1971.
28. Schramm B, Schmiedel H, Gehrman R, Bartl R, Ber. der Bunsen-Ges. für phys. Chem. 1977; **81**: 316.
29. Schmiedel H, Gehrman R, Schramm B, Ber. der Bunsen-Ges. für phys. Chem. 1980; **84**: 721.
30. Dillard DD, Waxman M, Robinson R L, J. Chem. Eng. Data. 1978; **23**: 269.
31. Patel MR, Joffrion LL, Eubank PT, AIChE J. 1988; **34**: 1229.
32. Whalley E, Schneider WG, Trans. ASME. 1954; **76**: 1001.
33. Trappeniers N J, Wassenaar T, Wolkers G J, Physica (Amsterdam) 1966; **32**: 1503.
34. Beattie J A., Brierley J S, Barriault R J, J. Chem. Phys. 1952; **20**: 1615.
35. Santafe J, Urieta J S, Gutierrez Losa C., Rev. Acad. Cienc. Exactas, Fis., Quim. Nat. Zaragoza 1976; **31**: 63.
36. Vogel E, Ber. der Bunsen-Ges. für phys. Chem. 1984; **88**: 997.
37. Kestin J, Ro S T, Wakeham WA, J. Chem. Phys. 1972; **56**: 4119.
38. Berg R F, Moldover M R, J. of Phys. and Chem. Ref. Data 2012; **41**: 043104.
39. Trappeniers NJ, Botzen A, van Oosten J, van den Berg HR, Physica 1965; **31**: 945.
40. Kestin J, Leidenfrost W, Physica 1959; **25**: 1033.
41. Wilhelm J, Vogel E, Int. J. Thermophys. 2000; **21**: 301.
42. Kalelkar AS, Kestin J, J. Chem. Phys. 1970; **52**: 4248.
43. Clarke AG, Smith EB, J. Chem. Phys. 1968; **48**: 3988.
44. Gough DW, Matthews G P, Smith EB, J. Chem. Soc., Far. Trans. 1 1976; **72**: 645.
45. Dawe RA, Smith EB, J. Chem. Phys. 1970; **52**: 693.
46. Maitland GC, Smith EB, J. Chem. Soc., Far. Trans. 1 1974; **70**: 1191.

47. Goldblatt M, Guevara FA, McInteer BB, Phys. Fluids 1970; **13**: 2873.
48. Kestin J, Knierim K, Mason EA, Najafi B, Ro ST, Waldman M, J. of Phys. and Chem. Ref. Data 1984; **13**: 223.
49. Kestin J, Paul R, Clifford AA, Wakeham WA, Physica A 1980; **100**: 349.
50. Assael MJ, Dix M, Lucas A., Wakeham WA, J. Chem. Soc., Far. Trans. 1 1981; **77**: 439.
51. Le Neindre B, Garrabos Y, Tufeu R, Physica A 1989; **156**: 512.
52. Faubert FM, Springer G S, J. Chem. Phys. 1972; **57**: 2333.
53. Jain P C., Saxena SC., J. Chem. Phys. 1975; **63**: 5052.
54. Hemminger W, Int. J. Thermophys. 1987; **8**: 317.
55. Hammerschmidt U, Int. J. Thermophys. 1995; **16**: 1203.
56. Suarez-Iglesias O., Medina I, de los Angeles Sanz M, Pizarro C., Bueno JL, J. Chem. Eng. Data 2015; **60**: 2757.
57. Trappeniers NJ, Michels JPJ, Chem. Phys. Lett. 1973; **18**: 1.
58. Paul R, Indian J. Phys. 1962; **36**: 464.
59. Saran A., Singh Y, Can. J. Chem. 1966; **44**: 2222.
60. Weissman S, DuBro GA, Phys. Fluids **13** (1970) 2689.
61. Benenson RE, Rimawi K, Chaitin M, Goldenberg S, Kaplan D, Am. J. Phys. 1976; **44**: 1089.
62. Srivastava BN, Paul R, Physica 1962; **28**: 646.
63. Ghimire S, Adhikari NP, J. Mol. Model. 2017; **23**: 94,.
64. Waldrop JM, Bo Song, Patkowski K, Wang X, J. Chem. Phys. 2015; **142**: 204307.
65. Aziz RA., Salman MJ., Chem. Eng. Comm. 1989; **78**: 153.
66. Sheng X, Zhu H, Zhang Z, Zhang D, Lu J, Xiao J, Int. J. Quant. Chem. 2019; **119**: e25800.
67. Jäger B, Hellmann R, Bich E, Vogel E, J. Chem. Phys. 2016; **144**: 114304.
68. Ogilvie JF., Wang FY.H., J. Mol. Struct. 1992; **273**: 277.
69. Tanaka Y, Yoshino K, Freeman DE, J. Chem. Phys. 1973; **59**: 5160.
70. Barker JA, Fisher RA., Watts RO, Mol. Phys. 1971; **21**: 657.
71. Peng JF., Li P, Ren J, Qiao LW, Tang KT, J. At. Mol. Sci., 2011; **2**: 289.
72. Tang KT, Toennies JP, J. Chem. Phys. 1984; **80**: 3726.
73. Fransson T, Rehn DR, Dreuw A., Norman P, J. Chem. Phys. 2017; **146**: 094301.
74. Thakkar A.J., Hettema H, PE.S. Wormer, J. Chem. Phys. 1992; **97**: 3252.
75. Monchick L, KS. Yun, EA Mason, J. Chem. Phys. 1963; **39**: 654.
76. Bich E, R Hellmann, E Vogel, Mol. Phys. 2008; **106**: 1107.
77. Chapman S, Cowling TG, The Mathematical Theory of Non-Uniform Gases, New York: Cambridge University Press; 1952.
78. Barocchi F, Zoppi M, In: Birnbaum G, editor. Phenomena Induced by intermolecular Interactions, New York, Plenum; 1985, p. 311.
79. Zoppi M, Moraldi M, Barocchi F, Magli R, Bafile U, Chem. Phys. Lett. 1981; **83**: 294
80. Chrysos M, Dixneuf S, J. Chem. Phys. 2005; **122**: 184315
81. Dixneuf S, Racht F, Chrysos M, J. Chem. Phys. 2015; **142**: 084302
82. Racht F, Dixneuf S, and Chrysos M, J. Chem.Phys. 2015; **142**: 174304
83. Dalgarno A., Kingston AE, Proc. R. Soc. A 1960; **259**: 424.
84. Maroulis G, J. Phys. Chem. A 2000; **104**: 4772.
85. El-Sheikh SM, Tabisz GC, Buckingham AD, Chem. Phys. 1999; **247**: 407.
86. Meinander N, Tabisz GC, Zoppi M, J. Chem. Phys. 1986; **84**: 3005.
87. Buckingham AD, Trans. Far. Soc. 1956; **52**: 1035.
88. Jansen L, Mazur P, Physica 1954; **21**: 193.
89. Moraldi M, Borysow A, Frommhold L, Chem. Phys. 1984; **86**: 339.
90. Meinander N, Penner AR, Bafile U, Barocchi F, Zoppi M, Shelton DP, Tabisz GC, Mol. Phys. 1985; **54**: 493.
91. Fakhardji W, Szabo P, El-Kader MSA, Gustafsson M, J. Chem. Phys. 2020; **152**: 234302.
92. Teboul V, Godet J-L, Le Duff Y, Appl. Spectros. 1992; **46**: 476.
93. Dixneuf S, Chrysos M, Racht F, J. Chem. Phys. 2009; **131**: 074304.
94. Chrysos M, Racht F, J. Chem. Phys. 2015; **143**: 174301.
95. Głaz W, Bancewicz T, Godet J-L, J. Chem. Phys 2005; **122**: 224323.

96. Głaz W, Bancewicz T, Godet J-L, Gustafsson M, Haskopoulos A., Maroulis G, J. Chem Phys 2016; **145**: 034303.
97. Godet J-L, El-Kader MSA, J. of Quant. Spectr. & Rad. Transf. 2019; **231**: 9.
98. Posch HA., Mol. Phys. 1982; **46**: 1213.
99. Meinander N, Semiclassical calculations of profiles of induced spectra, In: Tabisz GC, Neuman M N, editors. Collision- and Interaction-Induced Spectroscopy. NATO ASI series (Series C: mathematical and physical sciences), Dordrecht Springer; 1995: **452**: 507.
100. Bancewicz T, Chem. Phys. Lett. 1993; **213**: 363.
101. Levine HB, J. Chem. Phys. 1972; **56**: 2455.
102. Frommhold L, Collision-induced absorption in gases. Cambridge: Cambridge University Press; 1994.
103. Basile AG, Gray CG, Nickel BG, Poll JD, Mol. Phys. 1989; **66**: 961.
104. Głaz W, Yang J, Poll JD, Gray GC, Chem. Phys. Lett. 1994; **218**: 183.
105. Chrysos M, J. Phys. B. At. Mol. Opt. Phys. 2000; **33**: 2875.
106. Hartye RW, Gray CG, Poll JD, Miller MS, Mol. Phys. 1972; **29**: 825.
107. Balucani U, Tognetti V and Vallauri R, Phys. Rev. A 1979; **19**: 177.

## Figure captions

**Fig. 1.** Temperature dependence of the Krypton gas interaction pressure second virial coefficients  $B$  in  $\text{cm}^3 \text{mol}^{-1}$  versus temperature in K. Comparison is made with previously available experimental results [21-35]. The calculations were performed using the present BFW interatomic potential.

**Fig. 2.** Evolution of the ratio  $M_n^{\text{cal}}/M_n^{\text{exp}}$  of calculated to experimental depolarized moments when  $n$  varies from 1 to 4. Three anisotropy models (PM, MP2 and SCF [84]) and four intermolecular potential models (BFW in red, CCSD in blue, HFD in brown, MTT in indigo) are considered. Due to experimental uncertainties reported by DCR [93], the values of these ratios must be contained in the vicinity of one between the two black curves (dash and dash-dot).

**Fig. 3.** Comparison between the calculated depolarized CILS spectra of  $\text{Kr}_2$  at  $T=294.5$  K using different interatomic potentials (BFW: red; CCSD: blue; HFD-B: brown; MTT: indigo) and *ab initio* SCF pair polarizability anisotropy of Maroulis [84] with the experimental measurements. The bound and metastable pair contributions are represented by dashed lines.

**Fig. 4.** The same comparison as in Figure 3 between depolarized spectra generated by four potentials but for the MP2 pair polarizability anisotropy of Maroulis [84].

**Fig. 5.** The same comparison as in Figure 3 between depolarized spectra generated by four potentials but for the PM pair polarizability anisotropy defined by Eq. (18).

**Fig. 6.** Evolution of the ratio  $M_n^{\text{cal}}/M_n^{\text{exp}}$  of calculated to experimental isotropic moments when  $n$  varies from 1 to 4. Three trace models (MP, MP2 and SCF [84]) and four intermolecular potential models (BFW in red, CCSD in blue, HFD in brown, MTT in indigo) are considered. Due to experimental uncertainties reported in [94], the values of these ratios must be contained between the two black curves (dash and dash-dot).

**Fig. 7.** Comparison between the calculated isotropic CILS spectra of  $\text{Kr}_2$  at  $T=294.5$  K using different interatomic potentials (BFW: red; CCSD: blue; HFD-B: brown; MTT: indigo) and *ab initio* SCF pair polarizability trace of Maroulis [84] with the experimental measurements. The bound and metastable pair contributions are represented by dashed lines.

**Fig. 8.** The same comparison as in Figure 7 between isotropic spectra generated by four potentials but for the MP2 pair polarizability trace of Maroulis [84].

**Fig. 9.** The same comparison as in Figure 7 between isotropic spectra generated by four potentials but for the PM pair polarizability trace defined by Eq. (17).